Dual-Band Metasurface-Based Circularly Polarised Low-Profile Patch Antenna with Parasitic Elements

Qi Zheng[1,2*], Chenjiang Guo[1], Jun Ding[1], Guy A. E. Vandenbosch[2]

[1] School of Electronics and Information, Northwestern Polytechnical University, Xi'an China,
[2] ESAT-TELEMIC Research Division, Department of Electrical Engineering, KU Leuven, Leuven, Belgium.
[*] zhq930908@mail.nwpu.edu.cn

Abstract: A single-feed dual-band circularly polarised (CP) patch antenna is proposed. The antenna consists of a corner-truncated square patch antenna and a superstrate composed of a lattice of 2×2 metallic patches surrounded by parasitic elements. The driven patch generates one resonant mode. The metasurface with parasitic elements excites two additional resonant modes (TM10 and TM20). The combined resonances result in minimum axial ratio (AR) points, and a good dual-band CP operation is achieved. Simulations show that the antenna has a CP operating bandwidth of 40 MHz centered at 3.72 GHz (1.07%), and a CP operating bandwidth from 5.37 to 6.05 GHz (11.9%). The simulated gain is about 7.05-7.1 dBic for the low frequency band and 4.17-6.07 dBic for the high frequency band, respectively. Measurements and simulations are in good agreement.

1. Introduction

Dual- or multi-frequency operation antennas have received significant attention because they can meet the multiple demands in modern wireless communication systems [1]. It is also known that circularly polarized antennas have better robustness to multipath distortion and polarization mismatch losses between the transmitter and the receiver. Many typical techniques have been used to realize dual-band CP operation [1], such as stacked or parasitic patches, multiple feeds, etc.. However, these approaches always tend to yield a lower gain, a lower polarization purity, extra volume, or a complex feeding network. More recently, metamaterials, including composite right/left-handed transmission lines (CRLH TLs), artificial magnetic conductors (AMCs), electromagnetic band gaps (EBGs), high-impedance surfaces (HISs), reactive impedance surfaces (RISs), have been introduced in the design of conventional antennas [2-5] for size reduction, and wideband / multiple band operation. They provide several novel approaches to reach these goals [6-8].

These methods can be categorized into four types according to the placement of the metamaterials. The first type concerns the antenna backed by a metamaterial-based reflector. Dual-band/multiband antennas can be obtained by locating dual-band/wideband conventional antennas on a dual-resonant AMC [9-11]. A dual-band circularly polarised (CP) antenna was designed by utilizing the high band generated by the radiator and the low band caused by the AMC reflector [12].

The second type relates to placing metamaterials between the patch and ground plane. A multi-band patch antenna was presented by replacing the conventional substrate with a metamaterial structure [13]. Dual-band and dual-mode antennas with dual-polarization were realized by loading EBGs [14]. A dual-band microstrip antenna with omnidirectional and unidirectional CP radiation was designed by employing a CP patch radiator loaded with modified EBGs [15].

The third type considers patch radiator loading with metamaterials. For example, the complementary split ring resonator (CSRR) has been widely used in patch antennas for dual-band applications [16-20]. Epsilon negative transmission lines (ENTLs) [21, 22], CRLH TLs [23-29], and left-handed (LH) structures [30] were loaded in conventional antennas for dual-band/multi-band operation. These approaches achieve dual/multiple operating bands with dual/multiple modes effectively, but have a drawback, the narrow bandwidth.

The fourth type concerns integrating the metamaterial-based superstrate on top of the patch antenna. A one-dimensional EBG-based two layered superstrate with a positive reflection phase gradient in two bands was designed for a dual-band high-gain Fabry-Perot antenna [31], with a large volume. A metasurface was integrated with a dual-band patch antenna to reach a monopole-like pattern with a low profile [32]. However, it can be seen that most of the research referred to concerns linearly polarised (LP) radiation [31, 32]. In this paper, a dual-band compact CP antenna with a novel superstrate is presented. The superstrate consists of a metasurface with surrounding parasitic elements. The driven antenna is a corner-truncated square patch antenna. The proposed design achieves two resonant modes in the high frequency band by introducing a metasurface with parasitic elements while keeping the CP radiation of the driven patch antenna, offering a potential solution for dual-band communications. The paper is organized as follows: Section II presents the design and analysis of the proposed antenna. Section III gives the measured results of the fabricated prototype. Finally, Section IV concludes the work.

2. Design and analysis of the proposed antenna

2.1. Configuration

The schematic of the proposed dual-band CP patch antenna is shown in Fig. 1. It is composed of a metasurface consisting of 2×2 metallic square patches with surrounded parasitic elements printed on the top substrate, and a corner truncated square patch antenna printed on the bottom substrate. The unit cell patch of the metasurface has a

dimension a_1 and the patch of the parasitic element has a dimension a_2. The period dimension of both patches is p. The patch antenna is a square patch element ($l \times l$) with square truncations in two corners of size $b \times b$. Both substrates have a dielectric constant of 3.5 and a dielectric loss tangent of 0.003. The design is compact because no air gap is used between the superstrate and the patch element. Numerical simulations and optimizations have been carried out using CST Microwave Studio. The final parameters are: $p = 12$ mm, $a_1 = 10$mm, $a_2 = 11.5$mm, $L = 48$mm, $w_f = 3.5$mm, $l_f = 5$mm, $l = 17$mm, $b = 4.3$mm, $h_1 = h_2 = 1.5$ mm.

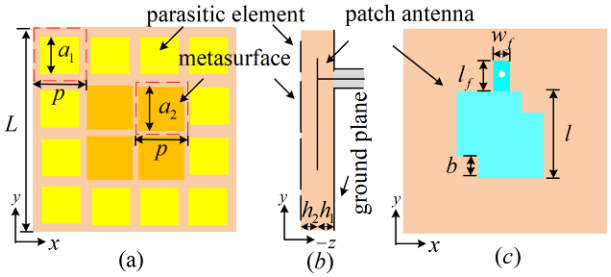

Fig. 1. *Schematic of the proposed antenna* ***(a)*** *top view,* ***(b)*** *side view,* ***(c)*** *patch antenna.*

2.2. Design process and performance

The design process of the proposed antenna is depicted in Fig. 2. Fig. 2(a) gives the schematic view of a traditional square patch antenna with two square truncated corners. The antenna is fed by a coaxial probe and an extended strip is used for better impedance matching. Fig. 2(b) shows a corner-truncated patch antenna covered with a metasurface-based superstrate. The metasurface consists of 2×2 square patches. Fig. 2(c) depicts the introducing of surrounding parasitic square patches.

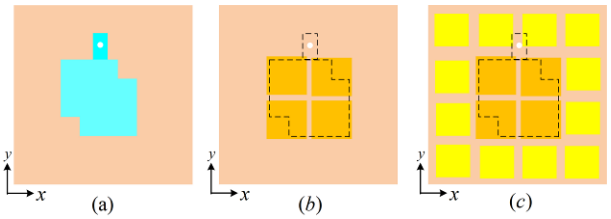

Fig. 2. *Design process of the antenna* ***(a)*** *driven patch antenna (Ant. 1),* ***(b)*** *metasurface-based antenna (Ant. 2),* ***(c)*** *metasurface-based antenna with parasitic elements (Ant. 3).*

The simulated S11 and AR of the driven patch antenna without the superstrate (Ant. 1), the topology with metasurface (2×2 square patches) only (Ant. 2), and the final topology with parasitic elements (Ant. 3) are compared in Fig. 3. The impedance matching and CP radiation performance of the driven patch antenna are not very good. A minimum S11 point occurs at 4.46 GHz with S11=-4.62 dB, and a minimum AR point occurs at 4.60 GHz with AR=16.89 dB (f_1). For the topology with the metasurface composed of 2×2 square patches, the impedance matching bandwidth is improved. A S11<-6 dB is obtained in the bands 3.61-4.11 and 5.27-5.56 GHz. The CP performance is not good in these bands, since minimum AR points are seen at 5.80, 6.00 and 6.80 GHz (f_{2a}, f_{2b}, and f_{2c}). The minimum AR point in the higher frequency region (f_{2d}) is not considered as it is caused by a high-order mode. For the final proposed topology, containing the outer smaller patches, the impedance matching in the higher band is further improved and an S11<-10 dB is obtained in the bands 3.60-3.93 GHz and 5.20-6.84 GHz. Three 3-dB AR bands are achieved and four minimum AR points at 3.72, 5.50, 6.05 and 6.50 GHz (f_{2a}, f_{2b}, f_{2c}, and f_{2d}) are generated. The highest resonance is caused by a high-order mode.

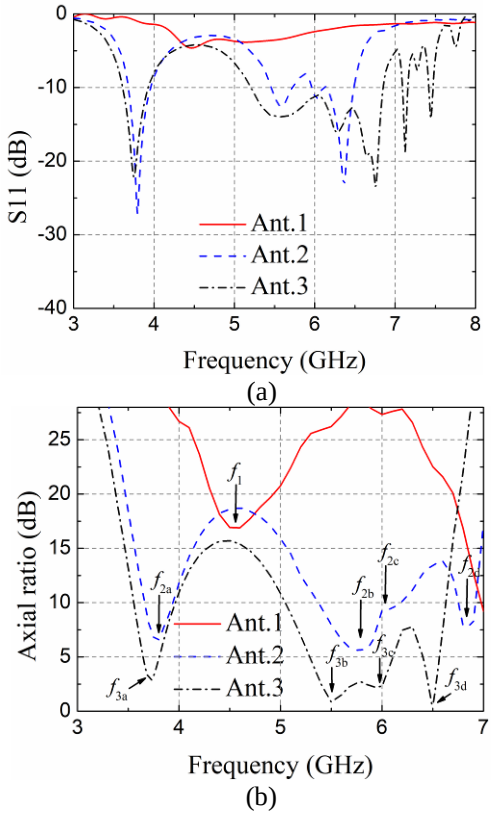

Fig. 3. ***(a)*** *S11,* ***(b)*** *AR of the antennas.*

In order to understand the effects of the superstrate, a qualitative analysis based on an equivalent circuit model is given in Fig. 4. After integrating the 2×2 square patches on the driven patch antenna, the frequency f_1 shifts to the lower one f_{2a} due to the capacitance (C_0) generated by the driven patch and top metasurface. Besides, two resonant modes (f_{2b} and f_{2c}) are excited. By employing parasitic unit cells, additional inductances (L_2) and capacitances (C_2) are introduced to further reduce the operating bands and improve CP performance.

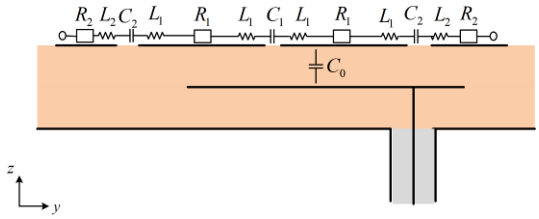

Fig. 4. *Additional inductances and capacitances introduced by the superstrate.*

2.3. Dual-band mechanism and analysis

According to the design process discussed above, the resonance in the first band comes from the driven patch, which is affected by the perturbation of the patch shape [1]. For the second band, the distribution of the total amplitude of the electric field and a qualitative sketch of the field lines at 5.5 and 6.05 GHz in the *yoz*-plane are presented in Fig. 5. It

is clearly seen that the electric field distributions generated by the metallic patches and driven patch antenna correspond to the TM_{10} and the antiphase TM_{20} modes, respectively. Similar to the wideband linearly polarised (LP) antenna of [11], which is also based on two resonant modes, the wide bands for the impedance matching and the 3-dB AR are ensured by the combination of the two resonant modes.

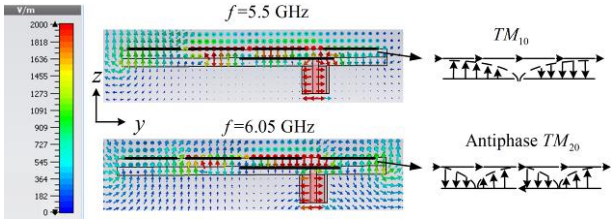

Fig. 5. *Electric field distribution and sketch diagram of resonant modes at 5.5 GHz and 6.05 GHz.*

A transmission-line model [1] can be used to further investigate the properties of the considered topology: a corner-truncated driven patch antenna covered by a metasurface and backed by a metallic ground plane. In a uniform transmission line loaded with a periodic unit cell, the surface wave is TM dominant and the resonances for the TM_{10} and the antiphase TM_{20} modes are roughly determined by the equations:

$$\beta_{m(TM_{10})} = \frac{\pi}{N \times p} \quad (1)$$

$$\beta_{m(TM_{20})} = \frac{2 \times \pi}{N \times p} \quad (2)$$

Where $\beta_{m(TM_{10})}$ and $\beta_{m(TM_{20})}$ represent the propagation constants of the corner truncated unit cell, N is the number of cells, and p is the period of the unit cell.

Fig. 6 gives the dispersion diagram of the metasurface unit cell. The resonant frequencies calculated by (1) and (2) for the TM_{10} and TM_{20} modes are 4.60 and 5.42 GHz, respectively. These two frequencies correspond to the frequencies 5.50 and 6.05 GHz in the second band of the proposed antenna. The discrepancy is mainly due to the finite number of unit cells and the influence of the parasitic patches.

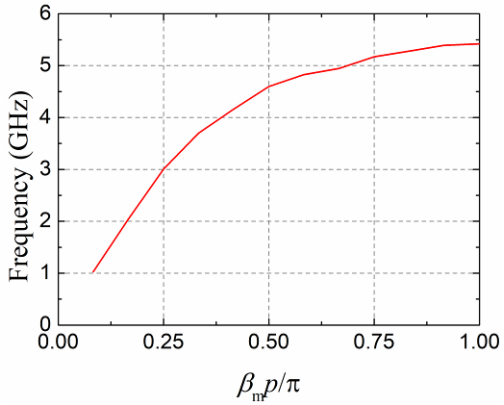

Fig. 6. *Dispersion diagram of the inner unit cell.*

The surface current distributions on the driven patch and the metasurface at the minimum AR points in the lower frequency band (corresponding to the broadside beam) and higher frequency band (corresponding to the off-broadside beam) are given in Fig. 7 and Fig. 8, respectively. In Fig. 7, on the driven patch the current flows vertically at feeding phase 0°, and horizontally at feeding phase 90°. This means that RHCP is generated by the patch. On the metasurface the current flows in nearly the same directions as the current on the driven patch but weaker magnitudes, reinforcing the CP behavior.

In Fig. 8, on the driven patch the current flows in the diagonal direction (from down left to top right) at feeding phase 0°, and from down right to top left at feeding phase 90°. Again, this means that CP is generated by the patch. On the metasurface the current flows in almost the opposite directions as the current on the driven patch, again reinforcing the RHCP behavior.

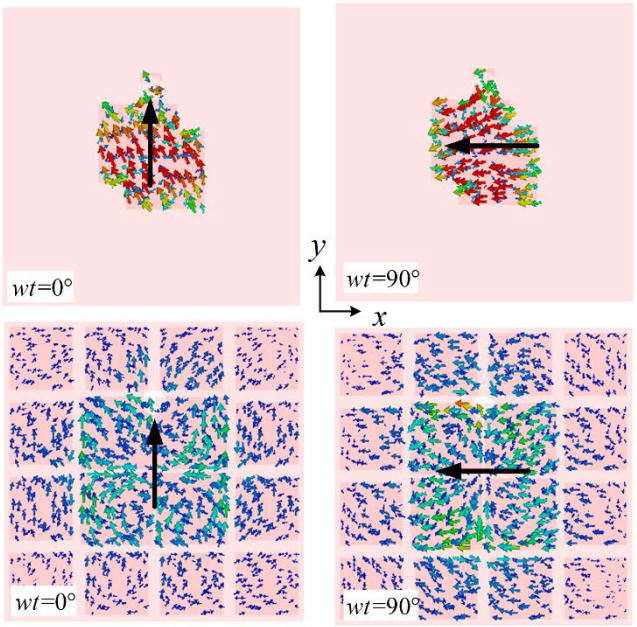

Fig. 7. *Surface currents at the minimum AR point in the lower band.*

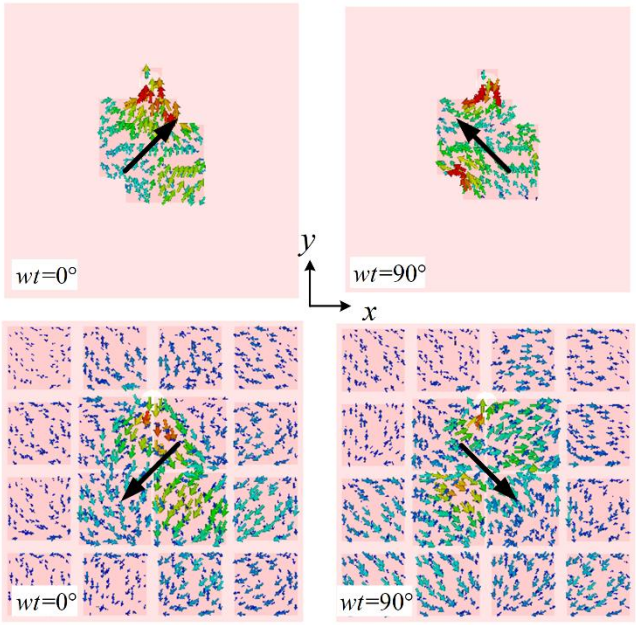

Fig. 8. *Surface currents at the minimum AR point in the higher band.*

2.4. Parametric studies

To understand the performance of the dual-band behavior, a parametric study has been carried out, investigating the effects of metasurface and parasitic elements. Comparing Fig. 9 (a) and (c), it is seen that changing the sizes of metasurface and parasitic unit cells has little influence on the low band, which verifies that the first resonant frequency is generated by the driven patch antenna. Besides, it can be seen that the metasurface unit cells play a more important role in the impedance matching in the high band. With the increase of the patch size a_1, the impedance matches better. The variation of the parasitic patch size a_2 has little influence on the impedance characteristics. According to Fig. 9(b) and (d), the variation of both the metasurface and parasitic elements has an impact on the axial ratio characteristics of the high band. Thus, the performance of the high band can be adjusted by optimizing the parameters of the superstrate independently with little impact on the low band.

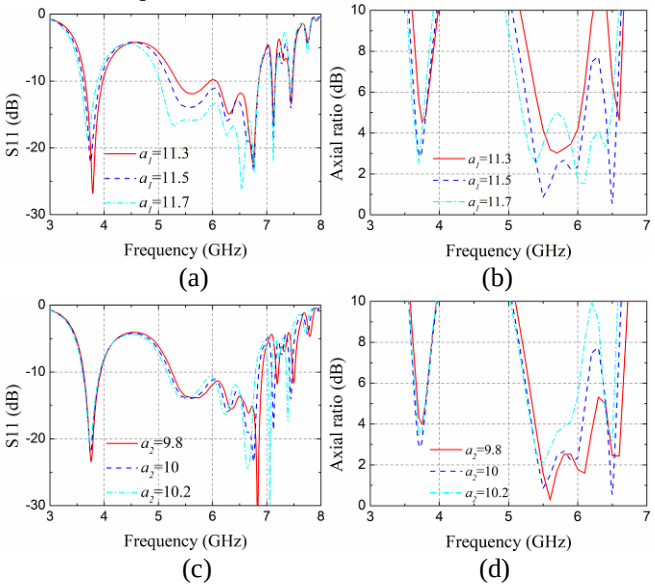

Fig. 9. *S11 and AR for different parameters* ***(a)*** *S11 with different a_1,* ***(b)*** *AR with different a_1,* ***(c)*** *S11 with different a_2,* ***(d)*** *AR with different a_2.*

3. Measurements

To verify the new concept, a prototype was fabricated and measured, as shown in Fig. 10(a). The measured impedance bandwidth is given in Fig. 8(b). It can be seen that in the measurements S11<-10 dB in the two bands of 3.60-4.15 GHz and 5.67-7.60 GHz, which is in good agreement with the simulations. Fig. 10(c) presents the measured and simulated AR and gain. The 3-dB AR bandwidths are 5.4-5.7 GHz and 50 MHz around 3.80 GHz, respectively. Meanwhile, the measured gain is about 7.10-7.20 dBic in the low band and 6.55-6.82 dBic in the high band, respectively. The frequency shift and other discrepancies between experiments and simulations are very reasonable, considering the normal fabrication tolerances and measurement errors.

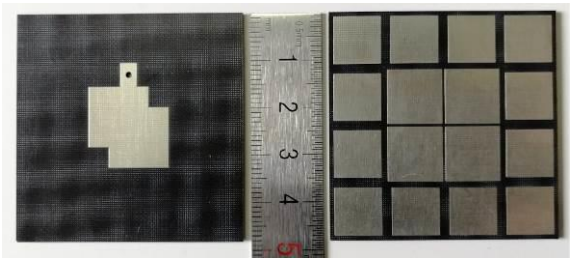

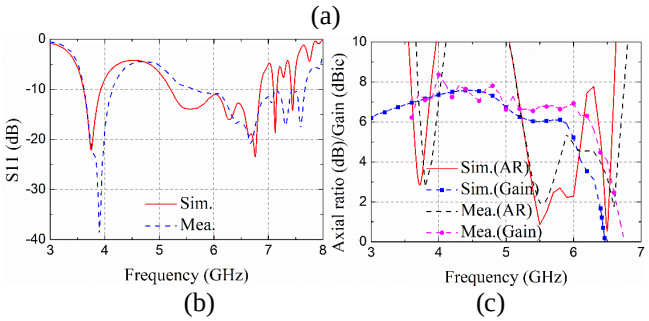

Fig.10. ***(a)*** *Front views of driven patch antenna and fabricated metamaterial. Simulated and measured results,* ***(b)*** *S11,* ***(c)*** *AR and gain.*

Measured and simulated radiation patterns in *xoz*-plane and *yoz*-plane at 3.75 and 5.5 GHz are shown in Fig. 11. The proposed antenna is RHCP. A good agreement between the measured and simulated results is obtained. A major disagreement is seen in the *xoz*-plane at the lower frequency, where the measured LHCP is significantly higher than the simulated one. Since the discrepancy is only in one plane, this could be caused by the unbalanced currents on the connected feed line and cables used in the measurement. The agreement of the RHCP in the two bands is very good. At 3.75 GHz, the experimental results show half-power beamwidths (HPBWs) of 90° and 85° in the *xoz*- and *yoz*-planes, respectively. At 5.5 GHz, over 75° HPBWs are obtained in the *xoz*- and *yoz*-planes. An off-broadside beam is observed in the high band due to the influence of the non-center feed of the driven patch antenna, but the AR along +*z* direction is still lower than 3 dB.

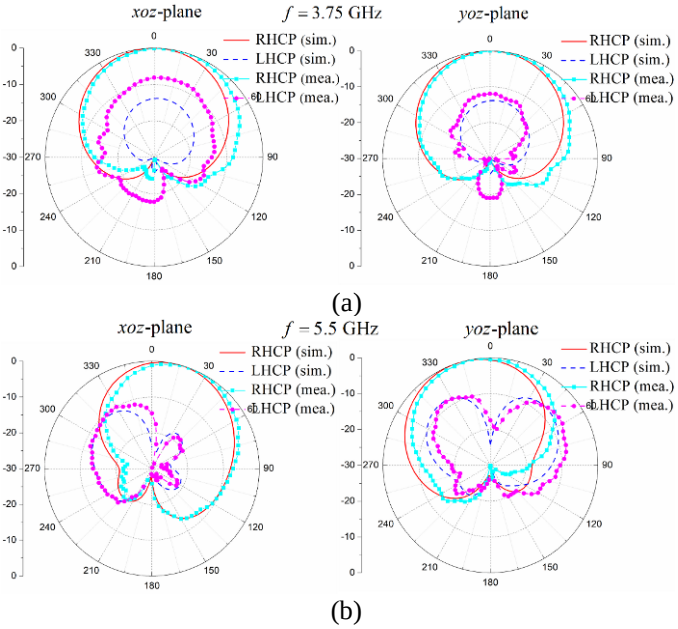

Fig.11. *Measured and simulated radiation patterns* ***(a)*** *3.75 GHz,* ***(b)*** *5.5 GHz*

The performance of several single-feed metamaterial-based dual-band CP antennas found in literature is overviewed in Table I. It can be concluded that the proposed antenna has a wider fractional bandwidth (FBW) for both impedance (IMBW) and AR (ARBW) in overall. Besides, comparing with dual-band metamaterial-based antennas with unidirectional radiation pattern, the proposed antenna has a

higher average radiation gain. The proposed antenna also has a higher gain compared with the unidirectional antenna presented in [12]. The cavity backed antenna in [19] produces on average a gain which is 1.6 dB higher, but at the cost of a significantly higher volume.

Table I Comparison of single-feed metamaterial-based dual-band CP antennas in literatures

Refs.	IMBW CF(GHz)/ FBW	ARBW CF(GHz)/ FBW	Polari-zation	Radiation Pattern	Gain (dBic)	Size(λ_0^3) and substrate	Method
[12]	1.2675/ 11.44%	1.23/ 3.25%	RHCP	Unidirectional	5.60	0.3485×0.348×0.047 $\varepsilon_r = 10.2$ and $\varepsilon_r = 2.2$	Radiator and AMC (TM01)
	1.6125/ 10.85%	1.565/ 3.83%	RHCP	Unidirectional	5.31		
[15]	1.789/ 1%	1.726/ Single frequency	CP	Omnidirectional	Not given	0.5753×0.5753×0.0144 $\varepsilon_r = 2.2$	Radiating patch and EBG (n=0,+1 mode)
	2.053/ 2%	2.032/ 1%	RHCP	Unidirectional			
[19a]	3.09/ 14.89%	3.205/ 3.2%	LHCP	Omnidirectional	5.9	0.7478×0.7478×0.0171 $\varepsilon_r = 4.4$	Corner-truncated square slot and split-ring resonator
	4.68/ 10.26%	4.85/ 4.2%	LHCP	Omnidirectional	6.2		
[19b]	3.115/ 17.66%	3.1/ 4.19%	LHCP	Unidirectional	8.4	0.7233×0.7233×0.125 $\varepsilon_r = 4.4$	[19a] with a backed cavity
	4.665/ 7.07%	4.75/ 2.11%	LHCP	Unidirectional	8.7		
[21]	1.85/ 0.54%	1.85/ >0.54%	LHCP	Omnidirectional	-0.24	0.2035×0.2035×0.0231 $\varepsilon_r = 2.2$	ENG TLs (n=0,+1 mode)
	2.8925/ 1.14%	2.89/ >0.49%	RHCP	Omnidirectional	-0.51		
[29]	2.385/ 6.3%	2.455/ 10.2%	LHCP	Omnidirectional	0.1	0.83×0.96×0.03 $\varepsilon_r = 4.4$	MNG TLs (n=0,+1 mode)
	3.46/ 8.1%	3.485/ 7.7%	LHCP	Omnidirectional	2.1		
This work	3.765/ 8.76%	3.72/ 1.07%	RHCP	Unidirectional	7.15	0.5952×0.5952×0.0372 $\varepsilon_r = 3.5$	Radiating patch and metasurface with parasitic elements
	6.02/ 27.24%	5.71/ 11.9%	RHCP	Unidirectional	6.68		

λ_0 - free space wavelength corresponding to the lowest resonant frequency

4. Conclusion

A single-feed dual-band CP patch antenna based on a metasurface with parasitic elements was proposed. The low band is generated by the driven patch antenna. Two minimum AR points in the high band are excited by the metasurface consisting of a lattice of 2×2 metallic patches. The parasitic elements are introduced to enhance impedance bandwidth and CP radiation. The performance in the high band can be adjusted independently. A prototype was fabricated and measured, showing a good agreement with simulations, and verifying the performance of the antenna. The dual-band CP operation covers the part of standard C-band transmit (5.850-6.425 GHz) and receive (3.625-4.200 GHz) frequency bands, which shows that the structure has the potential to be used in dual-band applications.

5. Acknowledgments

Authors thank the support from the China Scholarship Council (No. 201806290108).

6. References

[1] Gao S, Luo Q, Zhu F.: Circularly Polarized Antennas. John Wiley & Sons, 2014.

[2] Liu, W., Chen, Z. N., Qing, M.: 'Metamaterial-based low-profile broadband mushroom antenna'. *IEEE Trans. Antennas Propag*., 2014, 62, (3), pp 1165-1172

[3] Ta, S. X., Park, I.: 'Low-profile broadband circularly polarized patch antenna using metasurface'. *IEEE Trans. Antennas Propag*., 2015, 63, (12), pp 5929-5934

[4] Huang, Y., Yang, L., Li, J., Wang, Y., Wen, G.: 'Polarization conversion of metasurface for the application of wide band low-profile circular polarization slot antenna'. *Appl. Phys. Lett*., 2016, 109, (5), p 054101

[5] Chen, Q., Zhang H., Shao Y. J., Zhong, T.: 'Bandwidth and gain improvement of an L-shaped slot antenna with metamaterial loading. ' *IEEE Antennas Wireless Propag. Lett.* , 2018, 17, (8), pp 1411-1415

[6] Lee, K-F., Yang S. L. S., Kishk A. A.: 'Dual-and multiband U-slot patch antennas.' *IEEE Antennas Wireless Propag. Lett*., 2008, 7, pp 645-647

[7] Ferrero, F., Luxey, C., Jacquemod, G., Staraj, R.: 'Dual-band circularly polarized microstrip antenna for satellite applications. '*IEEE Antennas Wireless Propag. Lett.*, 2005, 4, (1), pp 13-15

[8] Gautam, A. K., Kumar, L., Kanaujia, B. K., Rambabu, K.: 'Design of compact F-shaped slot triple-band antenna for WLAN/WiMAX applications.' *IEEE Trans. Antennas Propag* , 2016, 64, (3), pp 1101-1105

[9] Kim, E.Y., Yoon, J.H., Yoon, Y.J., Kim, C.G.: 'Low profile dual-band reflector antenna with dual resonant AMC.' IEEE International Symposium on Antennas and Propagation (APSURSI) , 2011, pp. 1800-1803
[10] Lin, J., Qian, Z., Cao, W., Shi, S., Wang, Q., Zhong, W. 'A low-profile dual-band dual-mode and dual-polarized antenna based on AMC. ' *IEEE Antennas and Wireless Propag. Letters*, 2017, 16, pp 2473-2476
[11] Abbasi, N. A., Langley, R. J.: 'Multiband-integrated antenna/artificial magnetic conductor.' *IET Microwaves, Antennas & Propagation*. 2011, 5, (6), pp 711-717
[12] Ta, S. X., Park, I.: 'Dual-band operation of a circularly polarized radiator on a finite artificial magnetic conductor surface.' *J. Electromagnet. Wave.*, 2014, 28, (7), pp 880-892
[13] Weng, Z. B., Jiao, Y. C., Zhang, F. S., Song, Y., Zhao, G.: 'A multi-band patch antenna on metamaterial substrate.' J. Electromagnet. Wave.22, no. 2-3 (2008): 445-452
[14] Cao, W. Q., Zhang, B. N., Yu, T. B., Liu, A. J., Zhao, S-J., Guo, D-S., Song, Z-D.: 'Single-feed dual-band dual-mode and dual-polarized microstrip antenna based on metamaterial structure.' *J. Electromagnet. Wave*. 2011, 25, (13), pp 1909-1919
[15] Cao, W., Liu, A., Zhang, B., Yu, T., Qian, Z.: 'Dual-band spiral patch-slot antenna with omnidirectional CP and unidirectional CP properties.' *IEEE Trans. Antennas Propag.*,2013, 61, (4), pp 2286-2289
[16] Zhang, H., Li, Y.Q., Chen, X., Fu, Y.Q., Yuan, N.C.: 'Design of circular/dual-frequency linear polarization antennas based on the anisotropic complementary split ring resonator.' *IEEE Trans. Antennas Propag*., 2009, 57, (10), pp 3352-3355
[17] Zhou, L., Liu, S., Wei, Y., Chen, Y., Gao, N.: 'Dual-band circularly-polarised antenna based on complementary two turns spiral resonator.' *Electron. Lett.*, 2010, 46, (14), pp 970-971
[18] Yue, T., Jiang, Z. H., Panaretos, A. H., Werner, D. H.: 'A compact dual-band antenna enabled by a complementary split-ring resonator-loaded metasurface. ' *IEEE Trans. Antennas Propag.*, 2017, 65, (12), pp 6878-6888.
[19] Kandasamy, K., Majumder, B., Mukherjee, J., Ray, K. P.: 'Dual-band circularly polarized split ring resonators loaded square slot antenna.' *IEEE Trans. Antennas Propag*., 2016, 64, (8), pp 3640-3645.
[20] Saraswat, K., Harish, A. R.: 'Dual-band CP coplanar waveguide-fed split-ring resonator-loaded G-shaped slot antenna with wide-frequency ratio.' *IET Microwaves, Antennas & Propagation*., 2018, 12, (12), pp 1920-1925.
[21] Park, B.C., Lee, J.H.: 'Dual-band omnidirectional circularly polarized antenna using zeroth-and first-order modes.' *IEEE Antennas Wireless Propag. Lett.*, 2012, 11, pp 407-410
[22] Majedi, M.S., Attari, A.R.: 'Dual-band resonance antennas using epsilon negative transmission line.' *IET Microwaves, Antennas & Propagation*., 2013, 7, (4), pp 259-267
[23] Li, H., Zheng, Q., Ding, J., Guo, C.: 'Dual-band planar antenna loaded with CRLH unit cell for WLAN/WiMAX application.' *IET Microwaves, Antennas & Propagation*., 2017, 12, (1), pp 132-136
[24] Saurav, K., Sarkar, D., Srivastava, K.V.: 'Dual-polarized dual-band patch antenna loaded with modified mushroom unit cell.' *IEEE Antennas Wireless Propag. Lett.*, 2014, 13, pp 1357-1360
[25] Ko, S.T., Park, B.C., Lee, J.H.: 'Dual-band circularly polarized patch antenna with first positive and negative modes.' *IEEE Antennas Wireless Propag. Lett.*, 2013, 12, pp 1165-1168
[26] Zong, B., Wang, G., Zhou, C., Wang, Y.: 'Compact low-profile dual-band patch antenna using novel TL-MTM structures.' *IEEE Antennas Wireless Propag. Lett.*, 2015, 14, pp 567-570
[27] Ghaffarian, M. S., Moradi, G., Mousavi, P. 'Switchable dual/triple-band circularly polarised slot antenna by using artificial transmission line.' *IET Microwaves, Antennas & Propagation*, 2017, 11, (12), pp 1734-1741.
[28] Murugan, H. A., Reddy, G. B., Kumar, S.: 'Triple-Band zeroth order epsilon negative antenna using two pseudo-open termination unit cells for C-band applications.' *IEEE Antennas Wireless Propag. Lett.*, 2019, 18, (5), pp 1011-1015
[29] Chen, X., Han, L., Chen, X., Zhang, W. 'Dual-Band circularly polarized antenna using mu-negative transmission lines.' *IEEE Antennas and Wireless Propag. Lett.*, 2018, *17*, (7), pp 1190-1194.
[30] Herraiz-Martinez, F.J., Gonzalez-Posadas, V., Garcia-Munoz, L.E., Segovia-Vargas, D.: 'Multifrequency and dual-mode patch antennas partially filled with left-handed structures.' *IEEE. Trans. Antennas Propag.*, 2008, 56, (8), pp 2527-2539
[31] Zeb, B.A., Ge, Y., Esselle, K.P., Sun, Z., Tobar, M.E.: Tobar. 'A simple dual-band electromagnetic band gap resonator antenna based on inverted reflection phase gradient.' *IEEE. Trans. Antennas Propag.*,2012, 60, (10), pp 4522-4529
[32] Al-Zoubi, A., Yang, F., Kishk, A.: 'A low-profile dual-band surface wave antenna with a monopole-like pattern.' *IEEE. Trans. Antennas Propag.*, 2007, 55, (12), pp 3404-3412.